Progress In Electromagnetics Research, Vol. 152, 95–104, 2015

Extremely Sub-Wavelength Negative Index Metamaterial

Xu Zhang, Elvis Usi, Suhail K. Khan, Mehdi Sadatgol, and Durdu Ö. Güney

Abstract—We present an extremely sub-wavelength negative index metamaterial structure operating at radio frequency. The unit cell of the metamaterial consists of planar spiral and meandering wire structures separated by dielectric substrate. The ratio of the free space wavelength to unit cell size in the propagation direction is record breaking 1733 around the resonance frequency. The proposed metamaterial also possesses the most extreme refractive index of -109 that has been recorded to date. Underlying magnetic and electric response originate from the spiral and meandering wire, respectively. We show that the meandering wire is the key element to improve the transparency of the negative index metamaterial.

1. INTRODUCTION

Metamaterials were first coined in the late 1990s [1, 2]. Any material composed of usually periodic subwavelength structures to achieve a desired electromagnetic response that cannot be found in nature can be referred to as a metamaterial. Metamaterials offer a plethora of applications, such as flat lens [3], perfect lens [4], hyperlens [5–8], transformation optics [9–11], perfect absorbers [12, 13], optical analogue simulators [14, 15], compact antennas [16, 17], solar photovoltaics [18], and metaspacers [19], among others. Particularly, negative refractive index or double negative metamaterials [20–25] have been emerged as one of the most interesting classes of metamaterials due to the possibility of along-awaited diffraction unlimited imaging [4].

Despite a wide variety of applications, an important challenge faced today about metamaterials, especially at lower radio frequencies, is that the dimensions of a single unit cell element can become impractically large. Given the wavelengths at such low frequencies and typical sizes of the metamaterial elements on the order of $\sim \lambda_0/10$ to $\sim \lambda_0/100$, where λ_0 is the free space wavelength, the individual elements can be as large as hundreds of meters [26]. However, for real-world applications it is essential to miniaturize these metamaterial elements, which would require extremely sub-wavelength metamaterial designs.

Extremely sub-wavelength metamaterials are also relevant to applications such as controlling spontaneous emission [27–29] and quantum information processing [30–32, 33–40]. The light-matter interactions between free-space electromagnetic modes and quantum emitters are generally weak due to the small interaction cross-section of the latter. However, this can be directly challenged by using extremely sub-wavelength metamaterials, which can significantly enhance light-matter interactions by confining light and enhancing local fields in the metamaterial resonators.

Furthermore, it was predicted that the accuracy of the widely used effective parameter retrieval procedure [41–43] would be improved for extremely sub-wavelength metamaterials. The retrieved effective parameters are obtained by inverting transmission and reflection coefficients under homogeneous effective medium (HEM) approximation. Since the HEM approximation disregards the

Received 18 June 2015, Accepted 27 July 2015, Scheduled 29 July 2015

* Corresponding author: Durdu Öe Güeney (dguney@mtu.edu).

The authors are with the Department of Electrical and Computer Engineering, Michigan Technological University, 1400 Townsend Drive, Houghton, Michigan 49931, USA.

spatial dispersion, it usually results in non-physical negative imaginary parts in the retrieved constitutive parameters [43–49]. However, the influence of the spatial dispersion on the extremely sub-wavelength metamaterials diminishes and the accuracy of the HEM approximation improves.

Until now, the extremely sub-wavelength magnetic metamaterial has been designed with the unit cell size of about 2000 times smaller than the resonant wavelength [26]. A deeply sub-wavelength electric metamaterial has also been shown operating at GHz frequencies with the ratio of free space wavelength to unit cell size (i.e., referred to as λ_0/a ratio, where a is the unit cell size in the propagation direction) of about 70 [50]. Deeply sub-wavelength negative index metamaterials have been previously designed based on a lumped element with the unit cell size of only $\sim \lambda_0/75$ at 400 MHz [51]. Available manufactured lumped circuit elements offer only limited and coarse values. Desired operating frequency still depends on geometric unit cell design. Losses associated with lumped elements and the difficulties with the modelling are other challenges. These are discussed in detail in [51]. Here, we propose an extremely sub-wavelength negative index metamaterial structure with λ_0/a ratio reaching above 1700 and the refractive index reaching around -109, surpassing the previously recorded most extreme refractive index of only 38.6 [52]. It is difficult to achieve extremely subwavelength negative index metamaterial due to the lack of extremely subwavelength metamaterial electric resonators. Here, we alleviate this problem by using an important strategy to reduce the effective plasma frequency of the metamaterial. This enables the metamaterial better impedance matched to free space. Such a strategy has not been applied to metamaterials before to achieve extremely subwavelength operation and an extreme refractive index.

The paper is organized as follows: In Section 2, we show the design of the structure along with the parameters. In Section 3, we present the effective parameters and explain the physical mechanisms behind the working principle. First, we calculate the retrieved effective parameters in Section 3.1. Then, we explain the magnetic response in Section 3.2. In Section 3.3, we describe how we achieve the required complementary electric response for negative index of refraction. Section 3.3 is divided into two parts. In Section 3.3.1, we discuss the drawback of commonly used straight continuous wire approach for the electric response. In Section 3.3.2, we describe meandering wire design and its advantage for the required electric response. Previously, we used meandering wires to design negative index [21] and hyperbolic metamaterials [53] for direct laser writing processes [54–56].

2. PHYSICAL GEOMETRY

The unit cell of the sub-wavelength negative index metamaterial structure consists of three layers. The front side and the back side of a dielectric slab are a planar spiral and a planar meandering wire, respectively (see Fig. 1). The square spiral design has 60 turns, line width $w_1 = 200\,\mu\text{m}$, line spacing $g = 20\,\mu\text{m}$, center spacing $s = 2\,\text{mm}$, and the thickness of the spiral is $35\,\mu\text{m}$. The meandering wire design has 128 periods, line width $w_2 = 50\,\mu\text{m}$, meandering length $l = 29\,\text{mm}$, $h = 120\,\mu\text{m}$, and the thickness of the wire is $35\,\mu\text{m}$. The dielectric slab is $203\,\mu\text{m}$ thick and is modeled with a permittivity of $\varepsilon = 2.60 + 0.04i$. The square spiral and the meandering wire are made of copper with a conductivity of $\sigma = 5.8 \times 10^7\,\text{S/m}$. The dimension of the unit cell size is $30\,\text{mm} \times 30\,\text{mm} \times 20\,\text{mm}$. We used finite integration method based CST Microwave Studio software package to perform the simulation. The s-parameters corresponding to the complex reflection and transmission coefficients were calculated by using a frequency domain solver. Then the effective medium parameters of the metamaterial structure were retrieved by using the s-parameters [41]. Perfect electric conductor and perfect magnetic conductor boundary conditions were used in the simulations for the xz-plane and the xy-plane, respectively. We verified using periodic boundary conditions that the electromagnetic field cannot distinguish the lack of mirror symmetry in this specific structure [21]. We defined the incident electric field ($\mathbf{E}$) along the y-axis to excite the parallel electric current oscillations in the meandering wire. Magnetic field ($\mathbf{H}$) was along the z-axis to excite the magnetic resonant mode of the square spiral, and the propagation direction ($\mathbf{k}$) was along the x-axis. We selected the tetrahedral meshes with an adaptive meshing method to accurately represent the model to be simulated.

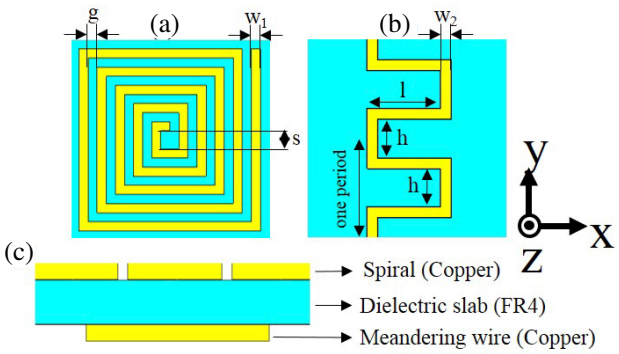

Figure 1. Schematic of the (a) spiral and (b) meandering wire structure with the geometric parameters indicated. (c) Side view of a small section of the structure showing material layers.

3. EFFECTIVE PARAMETERS AND PHYSICAL MECHANISMS

In this section, we show the results for the retrieved effective parameters of the metamaterial structure and explain the origins of magnetic and electric response of the proposed extremely subwavelength negative index metamaterial.

3.1. Effective Parameters

Figure 2(a) shows the resultant transmittance (T), reflectance (R), and absorbance (A). The spiral in the extremely subwavelength negative index metamaterial has 60 turns. In Fig. 2(b), we plot the retrieved effective refractive index, $n = n' + in''$. The negative refractive index bandwidth is 1.7 MHz (ranging from 5.6 MHz to 7.3 MHz). At 5.8 MHz, the real part of the refractive index reaches a record low of -108.6. Retrieved effective permittivity, $\varepsilon = \varepsilon' + i\varepsilon''$, and permeability, $\mu = \mu' + i\mu''$, are shown in Figs. 2(c) and (d), respectively. Notice that around 5.7 MHz, there is a magnetic resonance with a Lorentzian-like lineshape [57, 58]. The transmittance around resonance frequency is about 5%, the corresponding refractive index is -92, and the λ_0/a ratio is 1733. In the negative refractive index band, the transmittance is ranging from 4.5% to 7%, and the λ_0/a ratio is ranging between 1370 and 1782. The maximum figure of merit (FOM, defined as $-n'/n''$) is about 3 and more than 1 at $n' = -109$. These values are comparable with the low-loss (i.e., low absorption loss) metamaterials [20]. We should note that relatively poor impedance match here is a natural consequence of a large negative refractive index.

Figure 3 shows that both the impedance matching and the FOM can be further optimized by trading λ_0/a ratio and refractive index with improved transmittance resulting in an increase in the transmittance from 5% to 15% and a maximum FOM of about 4. The calculated absorption loss is about 1 dB/cm, which is on the same order as [51]. The final structure retains the record values of λ_0/a ratio of about 1000 and $n' = -56$.

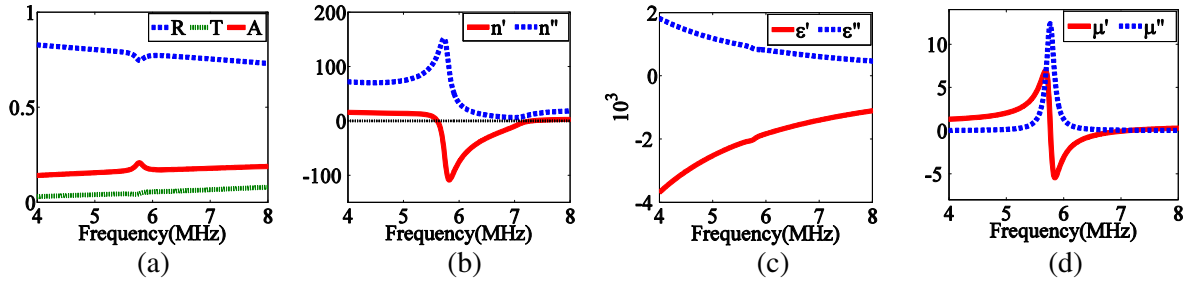

Figure 2. (a) Transmittance (T), reflectance (R), and absorbance (A) spectra. (b) Retrieved effective refractive index. (c) Effective permittivity, and (d) effective permeability. The spiral has 60 turns.

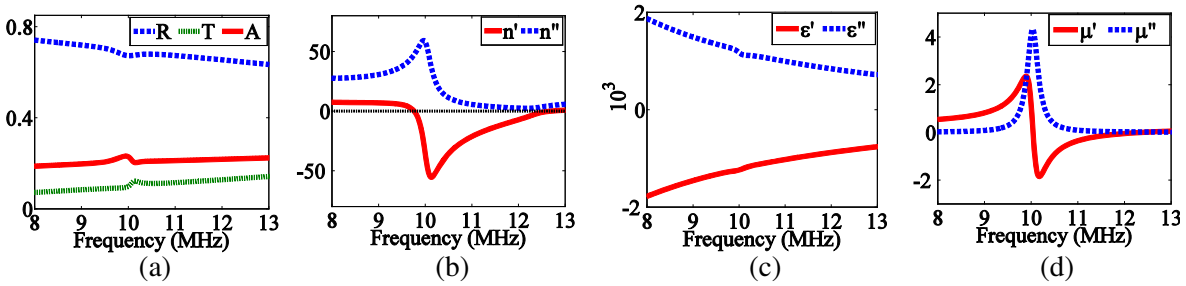

Figure 3. (a) Transmittance (T), reflectance (R), and absorbance (A) spectra. (b) Retrieved effective refractive index. (c) Effective permittivity, and (d) effective permeability. The number of turns in the spiral is reduced to 40 turns to blue-shift the operating frequency of the negative index metamaterial. This enables the metamaterial relatively better impedance matched to free space.

3.2. Magnetic Response

The magnetic response arises from the planar square spiral. The spiral can be considered as an LC resonator with the resonance frequency $\omega_0 = 1/\sqrt{LC}$, where L is the inductance due to the winding wires and C is the capacitance resulting from adjacent metallic windings [26]. Extremely sub-wavelength negative index metamaterials require sufficiently small magnetic resonance frequency. Therefore, L and C should be sufficiently large. By winding the significant length of wire into a small area, L is substantially increased. Additionally, decreasing the distance between the adjacent wires makes C increased. As shown in Fig. 2(d), the magnetic resonance frequency can be reduced down to around 5.7 MHz, while the unit cell size along the propagation direction is only 30 mm. This underlies the obtained large λ_0/a ratio.

Magnetic field and current density distributions near the magnetic resonance frequency for the structure considered in Fig. 2 are shown in Fig. 4. Fig. 4(a) shows the z component of magnetic field. The induced magnetic field is in the opposite direction with the incident magnetic field. In the central part of the spiral, the induced magnetic field is large enough to cancel the incident magnetic field. Therefore, the direction of the total magnetic field is dominated by the induced magnetic field. However, at the outer edge, the induced magnetic field cannot cancel the incident magnetic field, thus revealing the diamagnetic response [59, 60] of the metamaterial. A circular current flow can be observed in Figs. 4(b) and (c). The magnitude of the current density is shown in Fig. 4(d). It can be seen in Fig. 4(e) that the current density first increases with the distance from the center of the spiral and then decreases toward the edge. The direction of the induced magnetic field is perpendicular to the current flow. This verifies that the magnetic response originates from the spiral structure.

3.3. Electric Response

In the following we explain how we achieved the required electric response to obtain a measurable transmittance in the negative index band at an extremely subwavelength regime. We first point out the deficiency of commonly used straight continuous wire approach and then transform the straight wire into meandering wire for more favorable electric response.

3.3.1. Straight Continuous Wire

Initially, we used straight continuous wire on the backside of the dielectric substrate to obtain Drude-like negative permittivity. The wire length, width, and thickness were 30 mm, 200 μm, and 35 μm, respectively. We kept the geometric parameters for the spiral and the dielectric slab the same as in Fig. 2. However, the transmittance was almost zero in the resonance frequency range as shown in Fig. 5. Low transmittance is due to the impedance mismatch. Around the resonance frequency, the impedance of the structure is $z = 0.02 - i0.02$, while the impedance of the background is 1. Thus, to improve the transmittance, the impedance of the structure should be as close as possible to 1. At this frequency, the effective permittivity is $\varepsilon = -9111.7 - i5655.8$, and the effective permeability is $\mu = -4.7 + i6.7$.

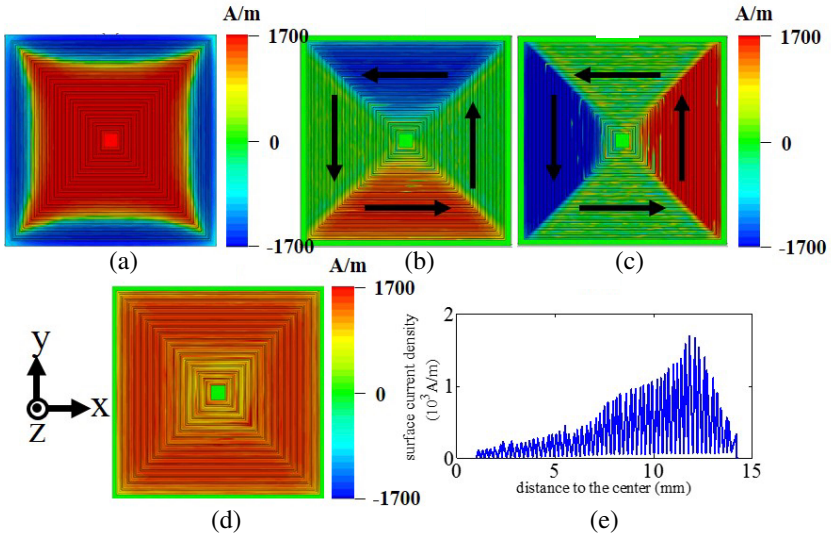

Figure 4. (a) Magnetic field at 5.7 MHz in the structure considered in Fig. 2. Colors show the z-component of magnetic field H_z. (b) Corresponding current density distribution. Colors show the x-component of current density J_x. (c) The same as (b) except that colors show the y-component of current density J_y. The complete loop current is indicated by black arrows overlaying the current density plots in (b) and (c). (d) The magnitude of the current density and (e) its distribution along a line extending from the center of the spiral to the edge.

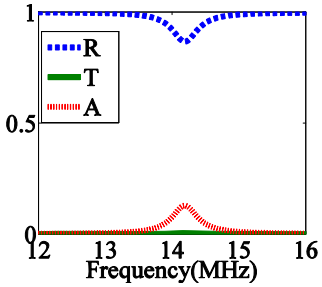

Figure 5. Transmittance (T), reflectance (R), and absorbance (A) spectra for the metamaterial with straight continuous wire on the back side of the substrate.

Negative imaginary part in ε is due to the deficiency of the HEM approximation at this wavelength (i.e., the structure is still not sufficiently subwavelength) [43–49].

It is clear that, ideally, we need to bring the complex permittivity to the same order as the complex permeability for the impedance match. This can be achieved if the operating frequency is close to the diluted plasma frequency. Therefore, we need to red-shift the plasma frequency as much as possible toward the magnetic resonance frequency. With the straight wire on the back side, the plasma frequency is equal to 943 MHz, while the magnetic resonance frequency is around 14 MHz. It is worth mentioning that the resonance frequency is blue shifted in Fig. 5 compared to Fig. 2, this is due to decreased overlap (or coupling), between the straight wire and the spiral.

3.3.2. Meandering Wire

Below we show that the plasma frequency can be significantly reduced if we transform the straight wire into a meandering wire. This is the reason why we adopted the meandering wire above to improve the transmittance of otherwise opaque metamaterial. Westart with presenting the results for induced electric current density and then explain in detail how the meandering wire approach gives more desirable electric response.

The parameters of the meandering wire are shown in Fig. 1. In Fig. 2(a), we can clearly see that the transmittance in the case of the meandering wire improves in comparison with the case for the straight wire. The impedance around the magnetic resonance frequency is $z = 0.06 - i0.04$. Although the impedance is only slightly improved, the transmittance reaches from almost zero to about 5%.

Because the induced non-resonant electric current on the meandering wire is much smaller than the induced resonant current on the spiral, it is difficult to clearly illustrate the non-resonant current. To address this problem, we first simulated the structure without spiral and obtained the electric current density shown in Fig. 6. Then, we compared the retrieved permittivity results with and without spiral and verified that the two plots are almost the same. This suggests that the current density distribution shown in Fig. 6 should also represent that of the negative index metamaterial structure discussed in Fig. 2.

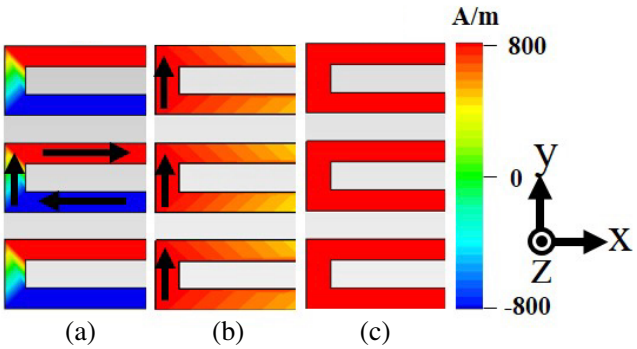

Figure 6. (a) Current density distribution on the meandering wire at 5.7 MHz. Colors show the x-component of the current density J_x. (b) The same as (a) except that colors show the y-component of current density J_y. The arrows overlaying the surface plots in (a) and (b) indicate the non-resonant current which flows along the meandering wire. (c) The magnitude of the current density.

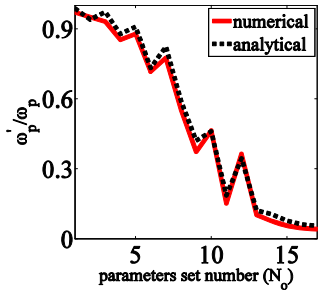

Figure 7. Graphical comparison of numerical and analytical results in Table 1 for ω'_p/ω_p.

Note that the induced non-resonant electric current density follows the trajectory of the meandering wire. As detailed below this is the essence of the reduced plasma frequency, hence improved transmittance.

The plasma frequency can be expressed as:

$$\omega_p = \sqrt{\frac{\rho_{eff} e^2}{\varepsilon_0 m_{eff}}} \tag{1}$$

where ρ_{eff} is the effective electron density, m_{eff} the effective mass of electrons, e the elementary charge, $e = 1.602 \times 10^{-19}$C. ε_0 is the electric permittivity for vacuum, $\varepsilon_0 = 8.854 \times 10^{-12}$ F/m. We first calculate ρ_{eff} and m_{eff} for both straight and meandering wires [61]. We define the width of the wires as w_2, the thickness as t, and the unit cell dimensions as $a \times a \times c$. For the straight wire, $\rho_{eff} = \rho w_2 t/ac$, where ρ is the electron density in the wire. $m_{eff} = e^2 N L_s$, where N is the total electron number per unit length, $\rho N = w_2 t$. L_s is the self-inductance per unit length, $L_s = (\mu_0/2\pi)\ln(a/w_2)$. For the meandering wire, both the effective electron density and mass change. Since meandering wire contains horizontal parts, the effective electron density becomes $\rho'_{eff} = \rho_{eff}(1 + 2lm/a)$, where m is the number of periods of the meandering wire and l is the length of the horizontal parts (see Fig. 1). On the other hand,we obtain the electron number per unit length and the self-inductance per unit length as $N' = N(1+2lm/a)$, $L'_s = L_s(1+2lm/a)$, respectively. Then, the effective mass of the electrons becomes $m'_{eff} = m_{eff}(1 + 2lm/a)^2$. Finally, we can relate the plasma frequency of these two wires by:

$$\frac{\omega'_p}{\omega_p} = \frac{1}{\sqrt{1 + \dfrac{2lm}{a}}} \tag{2}$$

Below we compare the CST simulation results with the analytical result. To obtain the optimal design for the meandering wire structure, we began with a small number of periods and l value, then gradually increased the number of periods and l. Table 1 shows 17 sets of parameters enumerated by N_o. Each set corresponds to one particular plasma frequency ω'_p. The numerical results for ω'_p/ω_p in Table 1 were obtained from the CST simulations, while the analytical results were obtained from Eq. (2). Both results are plotted in Fig. 7. The red solid line is the simulation result and black dashed line is the analytical result. We find an excellent agreement between both results. Thus, Eq. (2) and Fig. 7 show clearly that the plasma frequency can be significantly reduced by replacing the straight wire with the meandering wire. For the particular designs studied here, the plasma frequency reduces from 943 MHz to below 53 MHz. Increasing especially the number of periods and the length of horizontal parts plays an important role in the reduced plasma frequency by increasing the effective mass of the electrons. The transmittance can be increased by further optimization of the structure.

Table 1. Numerical and analytical results for ω_p'/ω_p using different meandering wire parameters; N_o is used to enumerate the parameter sets, m is the number of periods and l is the length of horizontal parts in nm.

N_o	m	l/2	numerical	analytical
1	1	0.4	0.97	0.9869
2	1	2	0.95	0.9303
3	2	0.4	0.93	0.9714
4	2	2	0.853	0.8776
5	4	0.4	0.878	0.9084
6	4	2	0.716	0.7319
7	8	0.4	0.775	0.8237
8	8	2	0.554	0.5912
9	8	5	0.373	0.4206

N_o	m	l/2	numerical	analytical
10	16	2	0.464	0.4602
11	16	10	0.1517	0.1858
12	32	2	0.3639	0.3442
13	32	10	0.102	0.1217
14	64	10	0.076	0.1051
15	64	14	0.056	0.0775
16	128	14	0.0457	0.0611
17	128	14.5	0.0412	0.0561

The geometrical parameters presented in Table 1 are the most effective geometrical parameters to reduce the plasma frequency as can be seen from Eq. (2). In Fig. 8 we show how these geometrical parameters affect the effective constitutive parameters, the attainable most extreme refractive index, and the corresponding FOM. Because the plasma frequency does not smoothly decrease with the geometrical parameters in Table 1 (see also Fig. 7), the plots in Fig. 8 also do not follow a smooth pattern. However, overall trend is that as the plasma frequency decreases ε' shifts upward, μ' becomes more negative, n' becomes less negative, and the FOM improves. Note that it is possible to obtain n' below -300 at the expense of lower FOM and higher impedance mismatch.

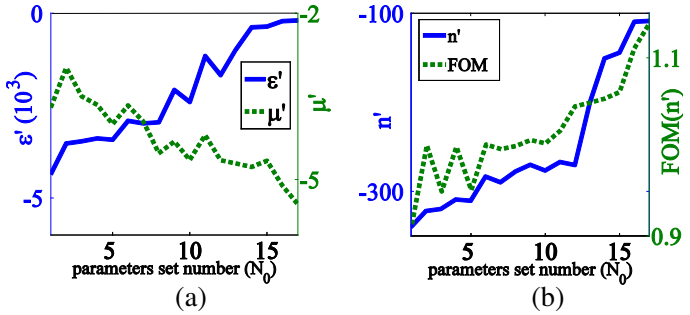

Figure 8. (a) Effective permittivity and permeability using the meandering wire parameters in Table 1. (b) The attainable most extreme refractive index and the corresponding FOM. The geometrical parameters for the spiral are the same as in Fig. 2.

4. CONCLUSION

In summary, we propose an extremely sub-wavelength negative index metamaterial structure operating at radio frequencies. Our design is within the limits of standard photolithography. The spiral in the metamaterial contributes to magnetic response and the meandering wire supports electric response. Meandering wire plays important role in improving the transparency of the metamaterial by reducing the diluted plasma frequency. The λ_0/a ratio is 1733 around the resonance frequency. Such an extremely large λ_0/a ratio for a negative index metamaterial has never been previously reported. Furthermore, the refractive index for the proposed metamaterial reaches down to -109. Regardless of the sign, this is the most extreme refractive index that has been reported to date. Extreme refractive index can be useful in transformation optics, high resolution imaging, enhanced light-matter interaction, miniaturization, and slow light applications. Our theoretical results are highly reliable due to the improved accuracy of the HEM approximation at extremely subwavelength dimensions.

ACKNOWLEDGMENT

This work was supported by the National Science Foundation under grant ECCS-1202443.

REFERENCES

1. Walser, R. M., "Electromagnetic metamaterials," *Complex Mediums II: Beyond Linear Isotropic Dielectrics*, A. Lakhtakia, W. S. Weiglhofer, and I. J. Hodgkinson, eds., *Proc. SPIE*, Vol. 4467, 1–15, 2001.
2. Cai, W. and V. Shalaev, *Optical Metamaterials: Fundamentals and Applications*, Academic, 2010.
3. Veselago, V. G., "The electrodynamics of substances with simultaneously negative values of ε and μ," *Sov. Usp.*, Vol. 10, 509–514, 1968.
4. Pendry, J. B., "Negative refraction makes a perfect lens," *Phys. Rev. Lett.*, Vol. 85, 3966, 2000.
5. Jacob, Z., L. V. Alekseyev, and E. Narimanov, "Optical hyperlens: Far-field imaging beyond the diffraction limit," *Opt. Express*, Vol. 14, 8247–8256, 2006.
6. Liu, Z., H. Lee, Y. Xiong, C. Sun, and X. Zhang, "Far-field optical hyperlens magnifying sub-diffraction-limited objects," *Science*, Vol. 315, 1686, 2007.
7. Zhang, X. and Z. Liu, "Superlenses to overcome the diffraction limit," *Nat. Mater.*, Vol. 7, 435–441, 2008.
8. Rho, J., Z. Ye, Y. Xiong, X. Yin, Z. Liu, H. Choi, G. Bartal, and X. Zhang, "Spherical hyperlens for two-dimensional sub-diffractional imaging at visible frequencies," *Nat. Commun.*, Vol. 1, 143, 2010.
9. Pendry, J. B., D. Schurig, and D. R. Smith, "Controlling electromagnetic fields," *Science*, Vol. 312, 1780–1782, 2006.
10. Leonhardt, U., "Optical conformal mapping," *Science*, Vol. 312, 1777–1780, 2006.
11. Schurig, D., J. J. Mock, B. J. Justice, S. A. Cummer, J. B. Pendry, A. F. Starr, and D. R. Smith, "Metamaterial electromagnetic cloak at microwave frequencies," *Science*, Vol. 314, 977–980, 2006.
12. Landy, N. I., S. Sajuyigbe, J. J. Mock, D. R. Smith, and W. J. Padilla, "Perfect metamaterial absorber," *Phys. Rev. Lett.*, Vol. 100, 207402, 2008.
13. Aydin, K., V. E. Ferry, R. M. Briggs, and H. A. Atwater, "Broadband polarization-independent resonant light absorption using ultrathin plasmonic super absorbers," *Nature Commun.*, Vol. 2, 517, 2011.
14. Guney, D. O. and D. A. Meyer, "Negative refraction gives rise to the Klein paradox," *Phys. Rev. A*, Vol. 79, 063834, 2009.
15. Smolyaninov, I. I. and E. E. Narimanov, "Metric signature transitions in optical metamaterials," *Phys. Rev. Lett.*, Vol. 105, 067402, 2010.
16. Bulu, I., H. Caglayan, K. Aydin, and E. Ozbay, "Compact size highly directive antennas based on the SRR metamaterial medium," *New J. Phys.*, Vol. 7, 223, 2005.
17. Odabasi, H., F. Teixeira, and D. O. Guney, "Electrically small, complementary electric-field-coupled resonator antennas," *J. Appl. Phys.*, Vol. 113, 084903, 2013.
18. Vora, A., J. Gwamuri, N. Pala, A. Kulkarni, J. M. Pearce, and D. O. Guney, "Exchanging ohmic losses in metamaterial absorbers with useful optical absorption for photovoltaics," *Sci. Rep.*, Vol. 4, 4901, 2014.
19. Aslam, M. I. and D. O. Guney, "On negative index metamaterial spacers and their unusual optical properties," *Progress In Electromagnetics Research B*, Vol. 47, 203–217, 2013.
20. Valentine, J., S. Zhang, T. Zentgraf, E. Ulin-Avila, D. A. Genov, G. Bartal, and X. Zhang, "Three-dimensional optical metamaterial with a negative refractive index," *Nature*, Vol. 455, 376–379, 2008.
21. Guney, D. O., Th. Koschny, M. Kafesaki, and C. M. Soukoulis, "Connected bulk negative index photonic metamaterials," *Opt. Lett.*, Vol. 34, 506–508, 2009.

22. Guney, D. O., Th. Koschny, and C. M. Soukoulis, "Intra-connected three-dimensionally isotropic bulk negative index photonic metamaterial," *Opt. Express*, Vol. 18, 12348–12353, 2010.
23. Garcia-Meca, C., J. Hurtado, J. Marti, A. Martinez, W. Dickson, and A. V. Zayats, "Low-loss multilayered metamaterial exhibiting a negative index of refraction at visible wavelengths," *Phys. Rev. Lett.*, Vol. 106, 067402, 2011.
24. Aslam, M. I. and D. O. Guney, "Surface plasmon driven scalable low-loss negative-index metamaterial in the visible spectrum," *Phys. Rev. B*, Vol. 84, 195465, 2011.
25. Aslam, M. I. and D. O. Guney, "Dual band double-negative polarization independent metamaterial for the visible spectrum," *J. Opt. Soc. Am. B*, Vol. 29, 2839–2847, 2012.
26. Chen, W.-C., C. M. Bingham, K. M. Mak, N. W. Caira, and W. J. Padilla, "Extremely sub-wavelength planar magnetic metamaterials," *Phys. Rev. B*, Vol. 85, 201104, 2012.
27. Decker, M., I. Staude, I. I. Shishkin, K. B. Samusev, P. Parkinson, V. K. A. Sreenivasan, A. Minovich, A. E. Miroshnichenko, A. Zvyagin, C. Jagadish, D. N. Neshev, and Y. S. Kivshar, "Dual-channel spontaneous emission of quantum dots in magnetic metamaterials," *Nat. Commun.*, Vol. 4, 2949, 2013.
28. Plum, E., V. A. Fedotov, P. Kuo, D. P. Tsai, and N. I. Zheludev, "Towards the lasing spaser: Controlling metamaterial optical response with semiconductor quantum dots," *Opt. Express*, Vol. 17, 8548–8551, 2009.
29. Moritake, Y., K. Nakayama, T. Suzuki, H. Kurosawa, T. Kodama, S. Tomita, H. Yanagi, and T. Ishihara, "Lifetime reduction of a quantum emitter with quasiperiodic metamaterials," *Phys. Rev. B*, Vol. 90, 075146, 2014.
30. Benz, A., S. Campione, S. Liu, I. Montaño, J. F. Klem, A. Allerman, J. R. Wendt, M. B. Sinclair, F. Capolino, and I. Brener, "Strong coupling in the sub-wavelength limit using metamaterial nanocavities," *Nat. Commun.*, Vol. 4, 2882, 2013.
31. Guney, D. O. and D. A. Meyer, "Creation of entanglement and implementation of quantum logic gate operations using a three-dimensional photonic crystal single-mode cavity," *J. Opt. Soc. Am. B*, Vol. 24, 283–294, 2007.
32. Guney, D. O. and D. A. Meyer, "Integrated conditional teleportation and readout circuit based on a photonic crystal single chip," *J. Opt. Soc. Am. B*, Vol. 24, 391–397, 2007.
33. Brune, M., F. Schmidt-Kaler, A. Maali, J. Dreyer, E. Hagley, J. M. Raimond, and S. Haroche, "Quantum Rabi oscillation: A direct test of field quantization in a cavity," *Phys. Rev. Lett.*, Vol. 76, 1800, 1996.
34. Brune, M., E. Hagley, J. Dreyer, X. Maitre, A. Maali, C. Wunderlich, J. M. Raimond, and S. Haroche, "Observing the progressive decoherence of the "meter" in a quantum measurement," *Phys. Rev. Lett.*, Vol. 77, 4887, 1996.
35. Turchette, Q. A., D. Kielpinski, B. E. King, D. Leibfreid, D. M. Meekhof, C. J. Myatt, M. A. Rowe, C. A. Sackett, C. S. Wood, W. M. Itano, C. Monroe, and D. J. Wineland, "Heating of trapped ions from the ground state," *Phys. Rev. A*, Vol. 61, 063418, 2000.
36. Raimond, J. M., M. Brune, and S. Haroche, "Manipulating quantum entanglement with atoms and photons in a cavity," *Rev. Mod. Phys.*, Vol. 73, 565, 2001.
37. Vandersypen, L. M. K., M. Steffen, G. Breyta, C. S. Yannoni, M. H. Sherwood, and I. L. Chuang, "Experimental realization of Shor's quantum factoring algorithm using nuclear magnetic resonance," *Nature*, Vol. 414, 883, 2001.
38. Kielpinski, D., C. Monroe, and D. J. Wineland, "Architecture for a large-scale ion-trap quantum computer," *Nature*, Vol. 417, 709, 2002.
39. Vandersypen, L. M. K. and I. L. Chuang, "NMR techniques for quantum control and computation," *Rev. Mod. Phys.*, Vol. 76, 1037, 2005.
40. Ospelkaus, C., U. Warring, Y. Colombe, K. R. Brown, J. M. Amini, D. Leibfreid, and D. J. Wineland, "Microwave quantum logic gates for trapped ions," *Nature*, Vol. 476, 181, 2011.
41. Smith, D. R., S. Schultz, P. Markos, and C. M. Soukoulis, "Determination of effective permittivity and permeability of metamaterials from reflection and transmission coefficients," *Phys. Rev. B*, Vol. 65, 195104, 2002.

42. Menzel, C., C. Rockstuhl, T. Paul, F. Lederer, and T. Pertsch, "Retrieving effective parameters for metamaterials at oblique incidence," *Phys. Rev. B*, Vol. 77, 195328, 2008.
43. Koschny, Th., P. Markos, E. N. Economou, D. R. Smith, D. C. Vier, and C. M. Soukoulis, "Impact of inherent periodic structure on effective medium description of left-handed and related metamaterials," *Phys. Rev. B*, Vol. 71, 245105, 2005.
44. Zhen, L., J. T. Jiang, W. Z. Shao, and C. Y. Xu, "Resonance-antiresonance electromagnetic behavior in a disordered dielectric composite," *Appl. Phys. Lett.*, Vol. 90, 142907, 2007.
45. Smigaj, W. and B. Gralak, "Validity of the effective-medium approximation of photonic crystals," *Phys. Rev. B*, Vol. 77, 235445, 2008.
46. Tserkezis, C., "Effective parameters for periodic photonic structures of resonant elements," *J. Phys: Condens. Matter*, Vol. 21, 155404, 2009.
47. Ludwig, A. and K. J. Webb, "Accuracy of effective medium parameter extraction procedures for optical metamaterials," *Phys. Rev. B*, Vol. 81, 113103, 2010.
48. Alu, A., "Restoring the physical meaning of metamaterial constitutive parameters," arXiv: 1012.1353, Submitted on Dec. 6, 2010.
49. Alu, A., "First-principles homogenization theory for periodic metamaterials," *Phys. Rev. B*, Vol. 84, 075153, 2011.
50. Kolb, P. W., T. S. Salter, J. A. McGee, H. D. Drew, and W. J. Padilla, "Extreme subwavelength electric GHz metamaterials," *J. Appl. Phys.*, Vol. 110, 054906, 2011.
51. Erentok, A., R. W. Ziolkowski, J. A. Nielsen, R. B. Greegor, C. G. Parazzoli, M. H. Tanielian, S. A. Cummer, B. Popa, T. Hand, D. C. Vier, and S. Schultz, "Lumped element-based, highly subwavelength, negative index metamaterials at UHF frequencies," *J. Appl. Phys.*, Vol. 104, 034901, 2008.
52. Choi, M., S. H. Lee, Y. Kim, S. B. Kang, J. Shin, M. H. Kwak, K.-Y. Kang, Y.-H. Lee, N. Park, and B. Min, "A terahertz metamaterial with unnaturally high refractive index," *Nature*, Vol. 470, 369–373, 2011.
53. Zhang, X., S. Debnath, and D. O. Guney, "Hyperbolic metamaterial feasible for fabrication with direct laser writing processes," *J. Opt. Soc. Am. B*, Vol. 32, 1013–1021, 2015.
54. Rill, M. S., C. Plet, M. Thiel, I. Staude, G. von Freymann, S. Linden, and M. Wegener, "Photonic metamaterials by direct laser writing and silver chemical vapour deposition," *Nat. Mater.*, Vol. 7, 543–546, 2008.
55. Gansel, J. K., M. Thiel, M. S. Rill, M. Decker, K. Bade, V. Saile, G. von Freymann, S. Linden, and M. Wegener, "Gold helix photonic metamaterial as broadband circular polarizer," *Science*, Vol. 325, 1513–1515, 2009.
56. Rill, M. S., C. E. Kriegler, M. Thiel, G. von Freymann, S. Linden, and M. Wegener, "Negative-index bianisotropic photonic metamaterial fabricated by direct laser writing and silver shadow evaporation," *Opt. Lett.*, Vol. 34, 19–21, 2009.
57. Guney, D. O., Th. Koschny, and C. M. Soukoulis, "Reducing ohmic losses in metamaterials by geometric tailoring," *Phys. Rev. B*, Vol. 80, 125129, 2009.
58. Zhang, S., W. Fan, K. J. Malloy, S. R. J. Brueck, N. C. Panoiu, and R. M. Osgood, "Near-infrared double negative metamaterials," *Opt. Express*, Vol. 13, 4922–4930, 2005.
59. Economou, E. N., Th. Koschny, and C. M. Soukoulis, "Strong diamagnetic response of in split-ringresonator metamaterials: Numerical study and two-loop model," *Phys. Rev. B*, Vol. 77, 092401, 2008.
60. Penciu, R. S., K. Aydin, M. Kafesaki, Th. Koschny, E. Ozbay, E. N. Economou, and C. M. Soukoulis, "Multi-gap individual and coupled split-ring resonator structures," *Opt. Express*, Vol. 16, 18131–18144, 2008.
61. Qin, G., J.-F. Wang, M.-B. Yan, W. Chen, H.-Y. Chen, and Y.-F. Li, "Lowering plasma frequency by enhancing the effective mass of electrons: A route to deep sub-wavelength metamaterials," *Chin. Phys. B*, Vol. 22, 087302, 2013.